

Higher-order calculations of electron-deuteron scattering in nuclear effective theory

Daniel R. Phillips

Department of Physics and Astronomy, Ohio University, Athens, OH 45701

Department of Physics, University of Washington, Box 351560, Seattle, WA 98195

Institute for Nuclear Theory, University of Washington, Box 351550, Seattle, WA 98195

Email: phillips@phy.ohiou.edu

Abstract

Motivated by recent advances in the application of effective field theory techniques to light nuclei we revisit the problem of electron-deuteron scattering in these approaches. By sidestepping problems with the description of electron-nucleon scattering data in effective field theories, we show that the effective theory expansion for deuteron physics converges well over a wide range of momentum transfers. The resultant description of the physics of the two-nucleon system is good up to virtual photon momenta of order 700 MeV.

PACS nos.: 12.39.Fe, 25.30.Bf, 21.45.+v

1 Introduction

Electron scattering from nuclei has a long and rich history. In impulse approximation the charge form factor probed in such experiments is the Fourier transform of the nuclear charge distribution, and so these measurements have often been regarded as independent tests of models of nuclear structure [1, 2]. In particular, the structure of nuclei with $A \leq 10$ can now be calculated *ab initio* from a given two- (and three-)nucleon interaction [3]. Calculations of electromagnetic form factors of these nuclei then reveal agreement with experimental data that is, in general, very good [4, 5]

Here we focus on the simplest non-trivial nucleus: deuterium. Elastic scattering of unpolarized electrons from deuterium results in an $O(\alpha^2)$ differential cross-section:

$$\frac{d\sigma}{d\Omega} = \frac{d\sigma}{d\Omega_{\text{Mott}}} \left[A(Q^2) + B(Q^2) \tan^2 \left(\frac{\theta_e}{2} \right) \right], \quad (1)$$

where θ_e is the electron scattering angle in the centre-of-mass frame of the collision, $q^2 = (p'_e - p_e)^2 \equiv -Q^2$ is the (negative) virtuality of the (single) photon exchanged between the electron and the nucleus, and $\frac{d\sigma}{d\Omega_{\text{Mott}}}$ is the Mott cross-section for electromagnetic scattering from a point particle of charge $|e|$ and mass M_d .

Deuterium is a spin-one nucleus and so has three independent form factors. These are usually denoted by G_C , G_Q , and G_M . They are related to Breit-frame matrix elements of the deuteron electromagnetic current, J_μ , through:

$$G_C = \frac{1}{3|e|} \left(\langle 1 | J^0 | 1 \rangle + \langle 0 | J^0 | 0 \rangle + \langle -1 | J^0 | -1 \rangle \right), \quad (2)$$

$$G_Q = \frac{1}{2|e|\eta M_d^2} \left(\langle 0 | J^0 | 0 \rangle - \langle 1 | J^0 | 1 \rangle \right) \quad (3)$$

$$G_M = -\frac{1}{\sqrt{2}\eta|e|} \langle 1 | J^+ | 0 \rangle \quad (4)$$

where we have labeled the deuteron states by the projection of the deuteron spin along the direction of the three-vector $\mathbf{p}'_e - \mathbf{p}_e$, and $\eta \equiv Q^2/(4M_d^2)$. When defined in this way these charge, quadrupole and magnetic form factors have the normalizations:

$$G_C(0) = 1, \quad (5)$$

$$G_Q(0) = Q_d, \quad (6)$$

$$G_M(0) = \mu_d \frac{M_d}{M}; \quad (7)$$

where $Q_d = 0.286 \text{ fm}^2$ [6] is the deuteron quadrupole moment, and $\mu_d = 0.85741$ [7] is the deuteron magnetic moment in units of nuclear magnetons.

The experimental quantities A and B can then be computed from theoretical models of deuterium, since

$$A = G_C^2 + \frac{2}{3}\eta G_M^2 + \frac{8}{9}\eta^2 M_d^4 G_Q^2, \quad (8)$$

$$B = \frac{4}{3}\eta(1 + \eta)G_M^2. \quad (9)$$

However, it was not until the development of experiments with polarized deuterium targets that it became possible to unambiguously extract both G_C and G_Q from electron-deuteron scattering data. The tensor-polarization observable, T_{20} , is related to the ratios

$$x = \frac{2}{3}\eta \frac{G_Q}{G_C}, \quad (10)$$

$$y = \frac{2}{3}\eta \left(\frac{G_M}{G_C}\right)^2 \left[\frac{1}{2} + (1 + \eta) \tan^2 \left(\frac{\theta_e}{2}\right) \right]; \quad (11)$$

by

$$T_{20} = \sqrt{2} \frac{x(x+2) + y/2}{1 + 2(x^2 + y)}, \quad (12)$$

and so a measurement of T_{20} , together with measurements of A and B allows an extraction of G_C and G_Q , and hence a complete test of our theoretical understanding of deuteron structure. Experiments over the last dozen years at Bates [8, 9], Novosibirsk [10, 11], NIKHEF [12, 13, 14], and Jefferson Laboratory [15] have measured T_{20} in electron-deuteron scattering, and so facilitated experimental determinations of the full set of deuteron structure functions over a kinematic range between $Q = 0$ and $Q = 1.5$ GeV [16, 17]. Modern nucleon-nucleon potentials, when combined with models for two-body contributions to the deuteron current, do a good job of reproducing this data (see, e.g. [18, 19, 20]). For a thorough status report on the subject of electron-deuteron scattering we refer to three recent reviews which discuss the subject [17, 21, 22].

In this paper we wish to address electron-deuteron scattering data in the framework of effective theories of deuteron dynamics. This approach (for recent reviews see Refs. [23, 24]) is based on the use of a chiral expansion for the physics of the two-nucleon system. Ultimately it shares many features with the more “traditional”, and very successful, potential models. However, as first suggested by Weinberg [25, 26, 27], this “nuclear effective theory” is based on a systematic chiral and momentum expansion for the the kernels of processes in the NN system. Thus, for electron-deuteron scattering we expand the deuteron current J_μ in operators which are ordered according to their chiral dimension, viz.:

$$J_\mu = e \sum_{i=1}^{\infty} c_i \frac{1}{\Lambda^{i-1}} \mathcal{O}_\mu^{(i)}, \quad (13)$$

where the operator $\mathcal{O}_\mu^{(i)}$ contains $i - 1$ powers of the small parameters p (the momentum of the nucleons inside deuterium), m_π , and Q . The numbers c_i are, *a priori*, assumed to

be of order 1, and Λ is the scale of chiral symmetry breaking: $\Lambda \sim 4\pi f_\pi, m_\rho, M$. Since the expectation value of p and the value of m_π are both much smaller than Λ it follows that, provided $Q < \Lambda$, and the cs really are of order one, this expansion should converge well. The expansion parameter $(p, Q, m_\pi)/\Lambda$ is denoted here by P .

The operators $\mathcal{O}_\mu^{(i)}$ and the coefficients c_i are constructed according to the well-established counting rules and Lagrangian of chiral perturbation theory [28]. Here we present results for G_C and G_Q up to order eP^3 , and results for G_M up to $O(eP^2)$. We go beyond the recent calculation of Ref. [29], which computed all three form factors only up to $O(eP^2)$. We also demonstrate that, provided single-nucleon structure effects are correctly included in the calculation, the nuclear effective theory is, in fact, much more accurate than the results of Ref. [29] might lead one to believe. Indeed, ultimately it describes all of the extant experimental data on G_C and G_Q out to momentum transfers of order 700 MeV.

This is done as follows. In Section 2 we sketch the derivation of J_μ from the counting rules of chiral perturbation theory, and give results for the current at leading order, $O(e)$, next-to-leading order $O(eP^2)$, and next-to-next-to-leading order, $O(eP^3)$. In Section 3 we will discuss the wave functions used in our calculation, and outline some of the issues associated with the desire for consistency between the deuteron current and the deuteron wave functions. In Section 4 we will present our results for G_C , G_Q , and G_M , as well as results for the deuteron's static properties μ_d , Q_d , and the deuteron charge radius. We conclude in Section 5.

2 The deuteron current

The heavy-baryon chiral perturbation theory (HB χ PT) Lagrangian is organized according to the powers of P which appear in the classical Lagrange density. The pieces of the leading-order ($O(P)$) heavy-baryon Lagrangian relevant to the computation to be presented here are:

$$\mathcal{L}_{\pi N}^{(1)} = N^\dagger (iv \cdot D) N + g_A N^\dagger u \cdot S N, \quad (14)$$

with:

$$D_\mu = \partial_\mu - \frac{ie}{2}(1 + \tau_3)A_\mu + \dots \quad (15)$$

$$u_\mu = iu^\dagger \partial_\mu U u^\dagger, \quad (16)$$

and v chosen to be $v = (1, 0, 0, 0)$, so that:

$$S = (0, \mathbf{S}); \quad \mathbf{S} = \frac{\boldsymbol{\sigma}}{2}, \quad (17)$$

We also choose the pion interpolating field such that:

$$u^2 = U = \exp\left(\frac{i\vec{\tau} \cdot \vec{\pi}}{f_\pi}\right). \quad (18)$$

A_μ is the photon field. Note that we have omitted some terms that are of higher-order in the pion field than we need for our calculation.

The part of $\mathcal{L}_{\gamma N}^{(2)}$ relevant for our calculation is the photon-nucleon piece. There we focus on the vertices, suppressed by order $p, Q/M$, that govern the coupling of E1 and M1 photons to the nucleon [30]:

$$\mathcal{L}_{\gamma N}^{(2)} = N^\dagger \frac{1}{2M} [(v \cdot D)^2 - D \cdot D] N - \frac{ie}{4M} N^\dagger [S_\mu, S_\nu] [(1 + \kappa_v)\tau_3 + (1 + \kappa_s)] F^{\mu\nu} N, \quad (19)$$

with $F_{\mu\nu}$ the electromagnetic field strength tensor. κ_s and κ_v are the isoscalar and isovector parts of the anomalous magnetic moment of the nucleon. These are known experimentally, and have the values -0.12 and 3.90 , respectively.

There is also an important term whose coefficient is entirely determined by reparameterization invariance. It occurs after the Foldy-Wouthysen transformation is used to eliminate the lower-component of the heavy-baryon field [30]:

$$\mathcal{L}_{FW}^{(2)} = -N^\dagger \frac{ig_A}{2M} \{S \cdot D, v \cdot u\} N. \quad (20)$$

Employing the definitions above, then reorganizing the result by eliminating total derivatives and using the nucleon equation of motion, leads to the piece relevant for our study:

$$\mathcal{L}_{\pi\gamma N}^{(2)} = \frac{eg_A}{2Mf_\pi} N^\dagger \tau^a \pi^a ((S \cdot \partial)v \cdot A) N. \quad (21)$$

The first occurrence of the finite electric radius of the isoscalar nucleon occurs in chiral perturbation theory as a coefficient in the Lagrangian $\mathcal{L}_{\gamma N}^{(3)}$. Similarly, the magnetic radius of the nucleon appears as a coefficient in $\mathcal{L}_{\gamma N}^{(4)}$. In both of these Lagrangians one also encounters terms arising from relativistic corrections to the single-nucleon four-current. The coefficients of these structures are determined by reparameterization invariance, and can be found by taking the relativistic current operator and using the standard procedure for generating the non-relativistic one-body current operator as an expansion in powers of p/M and Q/M (see, for instance [5, 31]).

Finally, in $\mathcal{L}^{(4)}$ we encounter a two-nucleon operator representing a magnetic photon coupling to the NN system [29, 32]:

$$\mathcal{L}_{\gamma NN_{\mathcal{M}}}^{(2)} = -ieL_2(N^\dagger [S_\mu, S_\nu] F^{\mu\nu} N)(N^\dagger N). \quad (22)$$

This short-distance two-body current will modify the magnetic moment of deuterium.

Similarly, in $\mathcal{L}_{\gamma NN}^{(3)}$ there is an operator which represents a quadrupole (E2) photon coupling to the NN system [33] and so modifies the deuteron quadrupole moment. At the same order there is also an operator which modifies the deuteron charge radius [33].

The vertices derived from the Lagrangians (14)–(22) are then used to draw all possible Feynman diagrams contributing to the process $\gamma^* NN \rightarrow NN$. A particular Feynman diagram then leads to an operator appearing in the sum (13). The power of P that this operator possesses is defined by considering all parts of the amputated Feynman diagram representing it, and multiplying together the “ P -scaling factors” of these separate pieces. These factors are defined as follows:

- A vertex from $L_{\pi N}^{(n)}$ contributes a factor of P^n .
- A vertex involving a photon from $L_{\gamma N}^{(n)}$, $L_{\gamma\pi N}^{(n)}$, or $L_{\gamma NN}^{(n)}$ contributes a factor of P^{n-1} [34].
- Each pion propagator contributes a factor of P^{-2} .
- Each nucleon propagator contributes a factor of P^{-1} .
- A two-body graph has an additional factor of P^3 .
- Each loop contributes a factor of P^4 .

We now discuss the charge and current operators in turn. Such a decomposition is, of course, not Lorentz invariant, so here we make this specification in the Breit frame, where the three-momentum of the deuteron and the nucleons is as shown in Fig. 1.

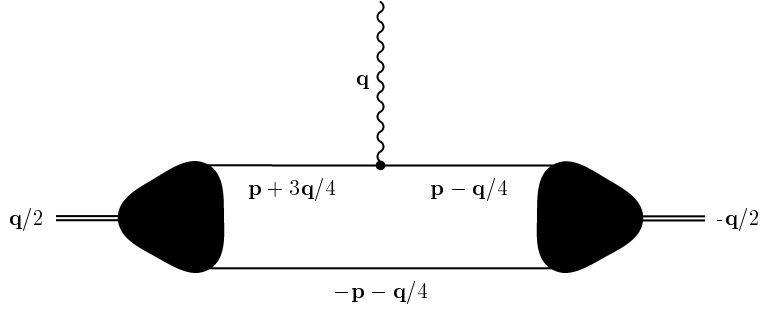


Figure 1: Three momenta of the deuteron, photon, and nucleons in the Breit frame for a generic one-body contribution to J_μ . This frame is chosen because in it the photon is purely space-like: $q = (0, \mathbf{q})$. Time runs from right to left.

Deuteron charge The vertex from $\mathcal{L}_{\pi N}^{(1)}$ which represents an A_0 photon coupling to the nucleon gives the leading-order (LO) contribution to J_0 :

$$J_0^{(0)} = |e|. \quad (23)$$

This is depicted in Fig. 2(a).

The most important correction to J_0 arises from the insertions in $\mathcal{L}_{\pi N}^{(3)}$ which generate the nucleon's isoscalar charge radius. This gives a result for J_0 through $O(eP^2)$:

$$J_{0\text{structure}}^{(2)} = |e| \left(1 - \frac{1}{6} \langle r_{Es}^2 \rangle Q^2 \right), \quad (24)$$

where $\langle r_{Es}^2 \rangle$ is the isoscalar charge radius of the nucleon, for which we adopt the value:

$$\langle r_{Es}^2 \rangle = (0.777 \text{ fm})^2. \quad (25)$$

(Note: $Q^2 = \mathbf{q}^2$ holds in the Breit frame.)

Also present at this order are relativistic corrections to the single-nucleon charge operator. To generate the “intrinsic” current operator which can be inserted between deuteron wave functions calculated in the two-nucleon center-of-mass frame we employ the formalism of Adam and Arenhövel, as described in Ref. [31]. The relativistic corrections then fall into two categories: corrections coming from the expansion of the relativistic single-nucleon current in powers of p/M , and corrections due to the necessity of boosting the deuteron wave function from the frame where $\mathbf{P} = \mathbf{0}$ to the frame where $\mathbf{P} = \pm \mathbf{q}/2$.

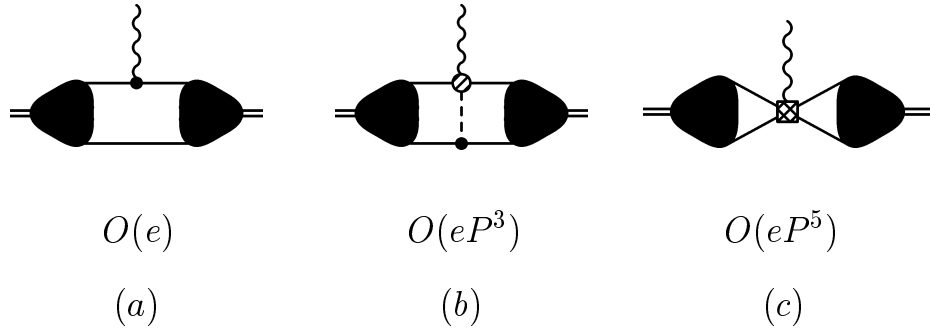


Figure 2: Diagrams representing the leading contribution to the deuteron charge operator [(a)], the leading two-body contribution to J_0 [(b)], and the dominant short-distance piece [(c)]. Solid circles are vertices from $\mathcal{L}_{\pi N}^{(1)}$, and the shaded circle is the vertex from $\mathcal{L}_{\gamma\pi N}^{(2)}$. The hatched square is a four-nucleon vertex from $\mathcal{L}_{\gamma NN}^{(3)}$.

When the calculation is organized in this way the dominant “relativistic effect” for momentum transfers of order 500 MeV is a shift in the length of \mathbf{q} . This “length contraction” accounts for a portion of the boost of the deuteron wave function (for details see Refs. [20, 31]). The net result is that whereas the leading-order form factor G_C can be represented as:

$$G_C^{(0)} = |e| \int \frac{d^3p}{(2\pi)^3} \psi^* \left(\mathbf{p} + \frac{\mathbf{q}}{2} \right) \psi(\mathbf{p}), \quad (26)$$

with ψ the deuteron wave function, at $O(eP^2)$ the expression is:

$$G_C^{(2)\text{boost}} = |e| \int \frac{d^3p}{(2\pi)^3} \psi^* \left(\mathbf{p} + \frac{\mathbf{q}}{2\sqrt{1+\eta}} \right) \psi(\mathbf{p}), \quad (27)$$

where $\eta = Q^2/(4M_d^2)$ was defined above. Here we have not reproduced the terms which scale as p/M , and we have not included the terms from Eq. (24). The sole effect written is

the one arising from the boost of the deuteron wave function, although all effects occurring at $O(eP^2)$ are included in our computation.

This completes the discussion of mechanisms contributing at $O(eP^2)$, or next-to-leading order. At $O(eP^3)$ —next-to-next-to-leading order—the Lagrangian (14) generates a tree-level two-body graph with an isoscalar structure, as shown in Fig. 2(b). This two-body contribution to J^0 was derived by Riska in Ref. [35], using an argument based on matching to relativistic Born graphs for pion electroproduction. Here it occurs in HB χ PT as a natural consequence of the Foldy-Wouthysen transformation which generates the relevant term in $\mathcal{L}^{(2)}$. Importantly, the nuclear effective theory also has the ability to organize the contribution of two-body contributions, such as this, relative to the contribution of one-body mechanisms.

Straightforward application of the Feynman rules for the relevant pieces of the HB χ PT Lagrangian gives the result for this piece of the deuteron current:

$$\langle \mathbf{p}' | J_0^{(3)}(\mathbf{q}) | \mathbf{p} \rangle = \tau_1^a \tau_2^a \frac{|e|g_A^2}{8f_\pi^2 M} \left[\frac{\sigma_1 \cdot \mathbf{q} \sigma_2 \cdot (\mathbf{p} - \mathbf{p}' + \mathbf{q}/2)}{m_\pi^2 + (\mathbf{p} - \mathbf{p}' + \mathbf{q}/2)^2} + (1 \leftrightarrow 2) \right], \quad (28)$$

where \mathbf{p} and \mathbf{p}' are the (Breit-frame) relative momenta of the two nucleons in the initial and final-state respectively [36].

The short-distance two-body currents that contribute to $\langle r_d^2 \rangle$ and Q_d are depicted in Fig. 2(c). They do not give a contribution until $O(eP^5)$. This suggests that the charge operator is not particularly sensitive to short-distance physics, since two-body effects of range $1/\Lambda$ are suppressed by five powers of P relative to the LO result.

Deuteron three-current The counting for the isoscalar three-vector current \mathbf{J} was already considered in detail by Park and collaborators [37]. \mathbf{J} begins at $O(eP)$. There the operator derived from $\mathcal{L}_{\gamma N}^{(2)}$ is:

$$\mathbf{J}^{(1)} = |e|(\mathbf{p} + \mathbf{q}/2)/M + i\mu_S \boldsymbol{\sigma} \times \mathbf{q}, \quad (29)$$

where $\mathbf{p} - \mathbf{q}/4$ is the momentum of the struck nucleon, as shown in Fig. 1, and μ_S is the isoscalar magnetic moment of the nucleon, whose value we take to be $\mu_S = 0.88|e|/(2M)$.

As in the case of J_0 , there are finite-size and relativistic corrections to Eq. (29) which are suppressed by two powers of P^2 . Thus, in this case they enter at $O(eP^3)$, and represent the NLO corrections to G_M . Loop graphs of the type depicted in Fig. 3(a) also enter at this order. However, it can be shown that the only effect of these loops on the isoscalar NN current is to renormalize the magnetic moment of the nucleon: their isoscalar part does not have any q^2 dependence (an analogous argument is given for real photons in Ref. [37]).

At $O(eP^4)$ [NNLO] two kinds of magnetic two-body current enter the calculation. Park *et al.* have pointed out that when magnetic photons interact with deuterium there is a

single-nucleon $\gamma\pi$ contact term in $\mathcal{L}_{\pi\gamma N}^{(3)}$ [37]. The coefficient of this portion of the chiral Lagrangian was fixed in Ref. [37] using the KSRF relation and a resonance-saturation hypothesis. Alternatively, this coefficient could also be fixed by comparison to data—at least in principle. In either case this $\gamma\pi NN$ vertex generates a pion-range two-body current with a coefficient that is undetermined *a priori*, as shown in Fig. 3(b).

Meanwhile, a number of authors [29, 32, 33, 37, 38], have pointed out that the short-distance two-body operator from the Lagrangian in Eq. (22) contributes to \mathbf{J} at $O(eP^4)$. It generates a “short-range” exchange-current contribution to G_M (see Fig. 3(c)). Since this is only suppressed by P^3 relative to the leading contributions to G_M we would expect G_M to be markedly more sensitive to details of the short-distance physics than G_C . Given the presence of two undetermined parameters at NNLO in \mathbf{J} we will only examine the leading and next-to-leading order predictions of the nuclear effective theory for G_M .

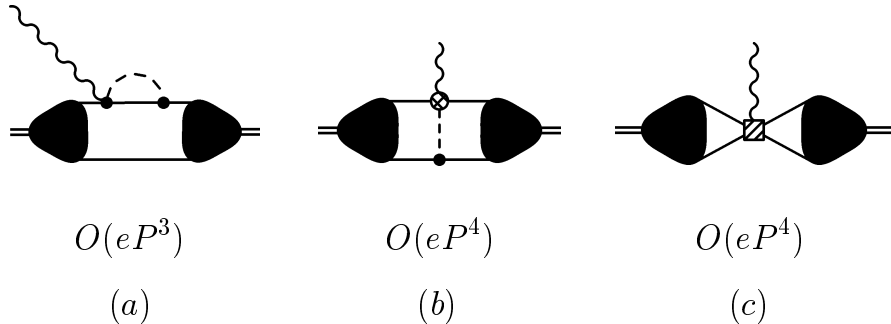


Figure 3: An $O(eP^3)$ loop diagram which ultimately does not generate q^2 -dependence in the nucleon isoscalar form factor [(a)], and two contributions of order $O(eP^4)$ [(b) and (c)]. The hatched circle is a vertex from $\mathcal{L}_{\pi\gamma N}^{(3)}$, while the shaded square is the vertex from $\mathcal{L}_{\gamma NN\mathcal{M}}^{(2)}$.

3 Deuteron wave functions

In order to define the computation completely it remains only to specify the deuteron wave functions which will be used for the evaluation of the matrix elements in Eqs. (2)–(4). Here we will use four different kinds of wave function:

1. A “strict” chiral perturbation theory wave function, as derived in Ref. [39]. We generally employ the NLO wave function, with the cutoff chosen to be $\Lambda = 600$ MeV. We also use Epelbaum et al.’s NLO wave function with $\Lambda = 540$ MeV for comparison.
2. The N²LO wave function of Ref. [40]. In this calculation a specific choice of cutoff is made, which allows for better accuracy in fitting NN phase shifts. Certain relativistic corrections to the NN potential are also included.

3. The wave functions derived in Ref. [41] by “integrating in” the one-pion exchange potential (OPEP) to a given radius R . These should be regarded as very simplistic potential models for deuterium. They are, however, designed to produce the correct values for the important deuteron properties A_S , A_D , and B , as well as to include the standard non-relativistic OPEP (with the “modern” coupling constant).
4. The deuteron wave function obtained using the Nijm93 meson-theoretic potential [42].

There is an important question of consistency with the current for all of these wave functions. In particular, it is well known that the charge contribution (28) is associated with so-called “relativistic corrections” to the one-pion-exchange potential. If $J_0^{(3)}$ and the terms in OPEP suppressed by p^2/M^2 relative to the leading behaviour are derived within a consistent framework then the results for deuteron form factors should be unitarily equivalent [43, 44, 45]. In fact, the authors of Ref. [39] did not consider “relativistic corrections” to one-pion exchange. They counted $M \sim \Lambda_\chi^2$ and so regarded the pieces of OPEP of relative order p^2/M^2 as being down by P^4 compared with the leading piece of the chiral NN potential. Indeed, none of the wave functions listed under numbers one, three, and four above include any “relativistic corrections” to one-pion exchange. Clearly a fully-consistent treatment of the deuteron current and NN potential in χ PT which incorporates what has been learned about unitary equivalence [43, 44, 45] is necessary if a definitive result is to be established for electron-deuteron scattering in the nuclear effective theory.

Here our goal is less ambitious. We take wave functions presently on the market and use the expansion for the deuteron current discussed in Sec. 2 to generate results for G_C , G_Q , and G_M . The error resulting from inconsistencies in this procedure can be assessed by comparing the results obtained with the wave functions of Refs. [39, 41, 42] to those found using the “Idaho” wave function of Ref. [40]. Of the wave functions used here, only the “Idaho” wave function includes the effect of relativistic corrections to one-pion exchange of the type associated by unitary equivalence with the two-body charge contribution (28).

4 Results

Strict chiral expansion The results of the leading-order (LO), next-to-leading order (NLO), and next-to-next-to-leading order calculations for G_C , using the NLO χ PT wave function of Ref. [39] with $\Lambda = 600$ MeV, are displayed in Fig. 4. Also shown there are data from the compilation [16]. The χ PT expansion for J_0 appears to be converging for $q \leq 600$ MeV, but it is not converging to the data. As was already observed in the NLO calculations of Walzl and Meißner [29], a strict chiral expansion of J^0 does a poor job of describing data on G_C for $Q^2 > 0.1$ GeV².

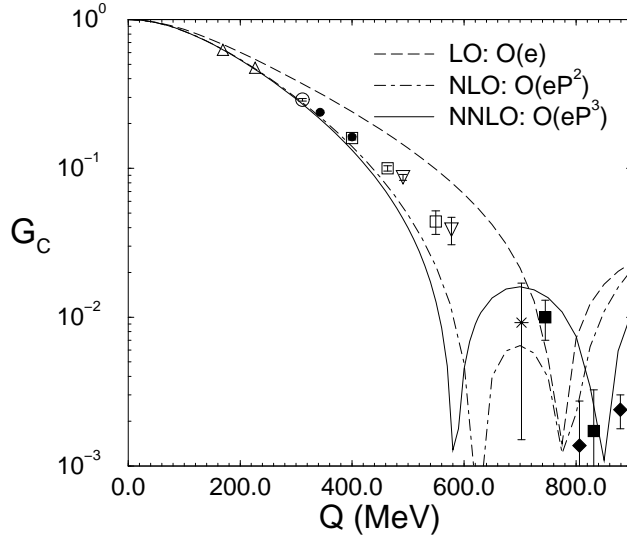


Figure 4: G_C as calculated in the strict χ PT expansion for J_0 at leading, next-to-leading, and next-to-next-to-leading order, plotted against $|\mathbf{q}|$. The experimental data is taken from the extraction of Ref. [16]: upward triangles represent data from the T_{20} measurement of Ref. [10], open circle [13], solid circle [8], open squares [14], downward triangles [11], star [12], solid squares [9], solid diamonds [15].

The reason for this failure can be traced to the isoscalar nucleon form factor obtained in χ PT [46]. That form factor is:

$$G_E^N(Q^2) = 1 - \frac{1}{6} \langle r_N^2 \rangle Q^2, \quad (30)$$

and it describes electron-nucleon scattering data only up to $Q^2 \sim 0.1 \text{ GeV}^2$. The inclusion of heavy mesons in the chiral lagrangian remedies this situation somewhat [47], but if we insist on a strict χ PT expansion—or even include explicit Delta degrees of freedom in the theory [48]—our description of electron-deuteron data will be limited by χ PT’s difficulty in describing single-nucleon isoscalar electromagnetic structure.

Factorization A solution to this problem is provided by the factorization of J_0 . Up to the order to which we work the deuteron charge operator can be written as the product of a piece that describes the current due to structureless nucleons and a nucleon-structure piece:

$$\langle \mathbf{p}' | J_0 | \mathbf{p} \rangle = (|e| \delta^{(3)}(p' - p - q/2) + \langle \mathbf{p}' | J_0^{(3)}(\mathbf{q}) | \mathbf{p} \rangle) G_E^N(Q^2) + O(eP^4). \quad (31)$$

(Relativistic corrections are not written here, but, at this order, factorization is also valid for them.)

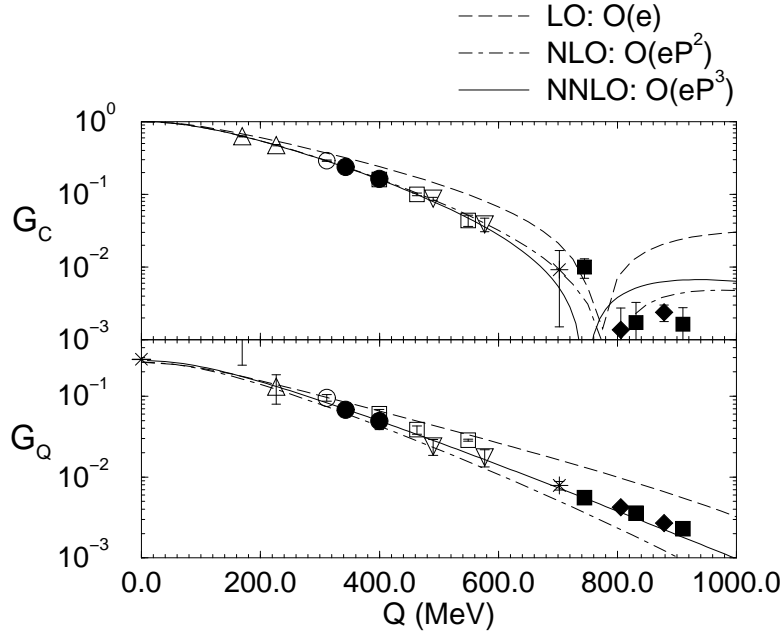


Figure 5: G_C and G_Q (in units of fm^2) calculated with nucleon structure effects included via factorization (at NLO and NNLO, LO is as before). The NLO χ PT deuteron wave function with $\Lambda = 600$ MeV was used. Legend as in Fig. 4.

Here we focus on the ability of nuclear effective theory to describe deuteron structure, and so we choose to apply the chiral expansion to the ratios of form factors:

$$\frac{G_C}{G_E^N} \quad \text{and} \quad \frac{G_Q}{G_E^N}. \quad (32)$$

To do this we compute the ratio J_0/G_E^N , i. e. the electric response of a deuterium nucleus containing structureless nucleons. Then, in order to compare with the compilation [16], the ratios (32) are multiplied by the parameterization of G_E^N found in Ref. [49]. The results obtained by this procedure are shown in Fig. 5. This time the expansion not only converges, provided that $Q \lesssim 700$ MeV, but also reproduces data on both G_C and G_Q in this range of Q .

Expanding the quantities (32) in the effective theory sidesteps χ PT's problems in describing isoscalar nucleon structure. We find that the chiral expansion for these ratios is in good agreement with data. Since these are the type of quantities which must be calculated in order to extract nucleon-structure information from deuteron data the results shown in Fig. 5 are quite encouraging in this regard.

Turning to the magnetic form factor, factorization also holds there, to the order to which we work, and so we compute the chiral expansion for the ratio J^+/G_M^N . Since we only calculate J^+ to NLO it is difficult to judge the convergence of the series, but the description of the data is quite good over the range $Q \lesssim 500$ MeV.

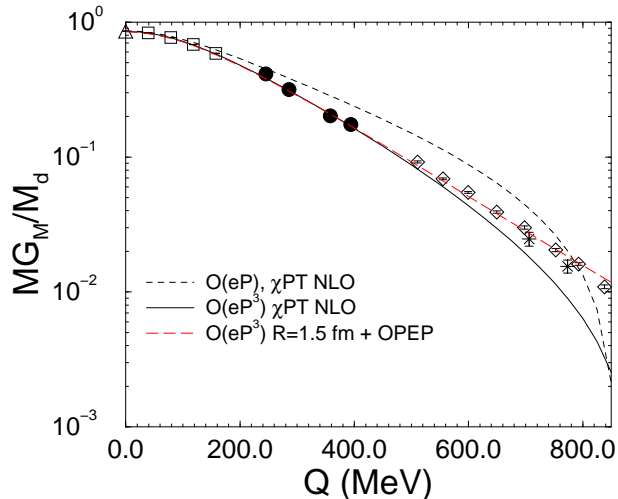


Figure 6: The deuteron magnetic form factor as calculated to LO with the χ PT NLO wave function (black short-dashed line) and NLO with the χ PT NLO wave function (solid black line) and the $R = 1.5$ fm + OPEP wave function (red long-dashed line). Factorization is used to include nucleon structure in the NLO results. Experimental data from deuteron magnetic moment, open triangle [7]; the parameterization of Ref. [17], open squares; and measurements of $B(Q^2)$: solid circles [50], open diamonds [51], and stars [52].

Estimating the size of short-distance effects In order to judge the sensitivity of this observable to short-distance effects, in Fig. 6 we also show the result for G_M obtained with a simple short-distance + OPEP wave function [41]. This wave function and the χ PT NLO wave function differ only at distances $r \ll 1/m_\pi$, and so the red-dashed line’s agreement with data to $Q \sim 900$ MeV should be regarded as fortuitous. From an EFT point of view, the difference between the red-dashed and solid curves in Fig. 6 is a short-distance effect. Such effects enter at NNLO in this observable, and so the sizable impact of physics at distances $r \sim 1/\Lambda$ on G_M that is seen in Fig. 6 is not surprising.

In contrast, short-distance contributions to G_C and G_Q do not occur until $O(eP^5)$. As with G_M , we can estimate their impact by computing the form factors with different deuteron wave functions—see Fig. 7. The results for G_C and G_Q are largely the same for $Q \lesssim 600$ GeV. The most noticeable difference occurs around the zero of G_C —a region where sensitivity to details of deuteron physics is well-established.

Intriguingly, the band representing different assumptions about short-distance physics is quite narrow out to values of $Q \gtrsim 800$ MeV when G_Q is considered. This suggests that the shape of G_Q is not strongly affected by short-distance physics, and higher-order corrections to it may well be small. (A similar conclusion was reached without the use of nuclear effective theory in Ref. [53].)

The curves of Figs. 5–7 are not, strictly speaking, predictions of χ PT for G_C and G_Q . In terms of the chiral expansion for these form factors a particular class of higher-order

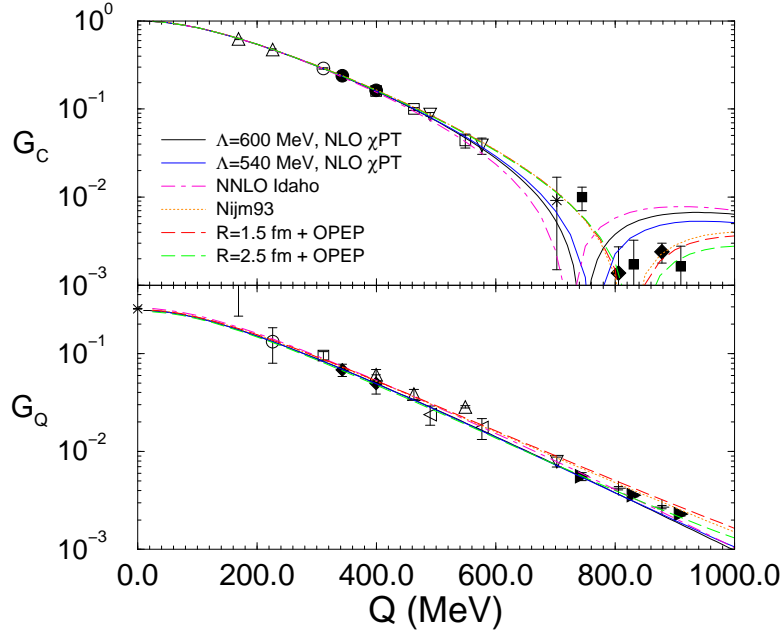


Figure 7: Results with different wave functions for G_C and G_Q (in units of fm^2). Solid black and blue lines are with wave functions from Ref. [39], purple dot-dashed with that of [40], dotted [42], and red and green long-dashed [41].

terms for electron-nucleon scattering have been resummed: the class of terms responsible for reproducing the “experimental” G_E^N . Nevertheless, the results of the procedure we have adopted show that nuclear effective theory does a good job of describing *deuteron* structure—and especially the deuteron charge distribution—out to surprisingly high momentum transfers.

Deuteron static properties: As far as deuteron static properties are concerned it is irrelevant how nucleon structure is included in the calculation. We have computed:

$$\langle r_d^2 \rangle \equiv -6 \left. \frac{dG_C}{dQ^2} \right|_{Q^2=0}, \quad (33)$$

when G_C is calculated with structureless nucleons. The result for $r_d \equiv \langle r_d^2 \rangle^{1/2}$ is shown in Table 1, together with results for μ_d and Q_d . Once again, the convergence of the expansion is very good, with the leading-order result capturing most of the physics of these static properties.

In order to assess the sensitivity of these quantities to short-distance effects we have computed r_d , μ_d , and Q_d with a variety of deuteron wave functions. The results are summarized in Table 2 and agreement with experimental data is very good. The $\sim 0.5\%$ discrepancy in r_d is certainly consistent with the expected size of the P^4 corrections

J_μ Order	r_d (fm)	μ_d (n.m.)	Q_d (fm ²)
LO	1.975	0.8591	0.2660
NLO	1.984	0.8531	0.2641
NNLO	1.987	Experiment	0.2764

Table 1: Deuteron static properties computed with the NLO χ PT wave function ($\Lambda = 600$ MeV) at LO, NLO, and NNLO. At NNLO μ_d can be exactly reproduced by adjusting the coefficient L_2 in Eq. (22). (The numerical error in each quantity is ± 1 in the last significant figure quoted.)

omitted here, while the $\sim 1\%$ discrepancy in μ_d is perhaps less than one would naively expect, given the that effects of relative order P^3 were not included in this computation of the deuteron’s magnetic moment.

	Experiment	Nijm 93	χ PT NLO $\Lambda = 600$ MeV	NNLO Idaho	OPEP + short $R = 1.5$ fm
A_S (fm ^{-1/2})	0.8846(8)	0.8842	0.869	0.885	0.8845
A_D/A_S	0.0256(4)	0.0252	0.0248	0.0245	0.0253
B (MeV)	2.224575(9)	Fit	2.161	Fit	2.2246
r_d (fm)	1.971(5)	1.979	1.987	1.984	1.975
μ_d (n.m.)	0.857406(1)	0.848	0.853	0.847	0.847
Q_d (fm ²)	0.2859(3)	0.280	0.276	0.291	0.280

Table 2: Deuteron static properties at NNLO (r_d and Q_d) and NLO (μ_d) for a range of deuteron wave functions. At NNLO μ_d can be reproduced exactly.

On the other hand, it is apparent that Q_d is much more sensitive to short-distance physics than either r_d or μ_d . Its value varies by about 5% between models with the same pion-range, but different short-distance, physics. The counterterm that would absorb this sensitivity is nominally of $O(eP^5)$, which we estimate to be almost ten times smaller than is necessary to absorb the variation seen in Table 2. Whether this counterterm should be promoted to a lower order—as has been argued in Refs. [33, 41]—cannot be properly determined until higher-order calculations of Q_d are performed and a systematic study of its renormalization-group evolution is made.

5 Conclusion

Chiral perturbation theory, applied to the deuteron four-current in the fashion suggested by Weinberg [25, 26, 27], produces an expansion in increasing powers of small momenta

(P) for the deuteron form factors G_C , G_Q , and G_M . However, this expansion fails to reproduce the experimental data at momentum transfers $Q \sim 300$ MeV [29]. The failure, however, lies not in χ PT’s description of *deuteron structure*, but with its difficulties in describing *isoscalar nucleon structure*. Applying a chiral expansion to the ratio of deuteron and nucleon form factors yields NNLO results for G_C and G_Q that agree with data to $Q \sim 700$ MeV. G_C and G_Q are also relatively insensitive to short-distance physics over this range.

The magnetic form factor, G_M , was computed up to NLO, and turns out to be more sensitive to short-distance physics. This result is anticipated within the effective theory, since short-distance two-body currents are suppressed by three powers of P relative to leading in G_M , but are down by two additional powers of P in G_C and G_Q .

Deuteron static properties are also well reproduced, although Q_d shows significant variability when different assumptions about deuteron short-distance physics are made. This may be associated with the “ Q_d -puzzle”: the inability of modern potential models to reproduce the experimental value for this quantity [5]. Any possible resolution of this puzzle within the nuclear effective theory will require the computation of higher-order effects in J_0 , including two-pion-exchange contributions to the deuteron four-current.

Acknowledgements

I gratefully acknowledge the hospitality of the Institute for Nuclear Theory, where part of this work was performed. I thank Jiri Adam, Tae-Sun Park, Martin Savage, and Steve Wallace for useful conversations on the subjects discussed here. Thanks also to Jacques Ball, Michel Garcon, and Ingo Sick for providing the parameterizations of the electron-deuteron scattering data, and to Charlotte Elster, Evgeni Epelbaum, Ruprecht Machleidt, and Vincent Stoks for supplying me with deuteron wave functions. This work was supported by the U. S. Department of Energy under grants DE-FG03-97ER41014, DE-FG02-93ER40756 and DE-FG02-02ER41218.

References

- [1] T. deForest and J. D. Walecka, *Adv. Phys.* **15**, 1 (1966).
- [2] C. J. Horowitz and B. D. Serot, *Nucl. Phys. A* **368**, 503 (1981).
- [3] S. C. Pieper, K. Varga and R. B. Wiringa, *Phys. Rev. C* **66**, 044310 (2002) [arXiv:nucl-th/0206061].
- [4] R. B. Wiringa and R. Schiavilla, *Phys. Rev. Lett.* **81**, 4317 (1998) [arXiv:nucl-th/9807037].

- [5] J. Carlson and R. Schiavilla, *Rev. Mod. Phys.* **70**, 743 (1998).
- [6] D. M. Bishop and L. M. Cheung, *Phys. Rev. C* **20**, 381 (1979).
- [7] I. Lindgren in *Alpha, Beta, and Gamma-Ray Spectroscopy*, Vol. 2, ed. K. Siegbahn (North Holland, Amsterdam, 1965).
- [8] M. E. Schulze *et al.*, *Phys. Rev. Lett.* **52**, 597 (1984).
- [9] M. Garcon *et al.*, *Phys. Rev.* **C49**, 2516 (1994).
- [10] V. F. Dmitriev *et al.*, *Phys. Lett. B.* **157**, 143 (1985).
- [11] R. Gilman *et al.*, *Phys. Rev. Lett.* **65**, 1733 (1990).
- [12] B. Boden *et al.* *Z. Phys.* **C49**, 175 (1991).
- [13] M. Ferro-Luzzi *et al.*, *Phys. Rev. Lett.* **77**, 2630 (1996).
- [14] M. Bouwhuis *et al.*, *Phys. Rev. Lett.* **82**, 3755 (1999).
- [15] D. Abbott *et al.*, *Phys. Rev. Lett.* **84**, 5053 (2000).
- [16] D. Abbott *et al.*, *Eur. Phys. J.* **A7**, 421 (2000).
- [17] I. Sick, *Prog. Part. Nucl. Phys.* **47**, 245 (2001) [arXiv:nucl-ex/0208009].
- [18] R. B. Wiringa, V. G. J. Stoks, and R. Schiavilla, *Phys. Rev. C* **51**, 38 (1995).
- [19] H. Arenhövel, F. Ritz, and T. Wilbois, *Phys. Rev.* **C61**, 034002 (2000).
- [20] R. Schiavilla and V. R. Pandharipande, *Phys. Rev.* **C65**, 064009 (2002).
- [21] M. Garcon and J. W. Van Orden, *Adv. Nucl. Phys.*, **26**, 293 (2001). [arXiv:nucl-th/0102049].
- [22] R. Gilman and F. Gross, *J. Phys. G* **28**, R37 (2002) [arXiv:nucl-th/0111015].
- [23] S. R. Beane *et al.*, in *At the frontier of particle physics, vol. 1*, edited by M. Shifman (World Scientific, Singapore, 2000).
- [24] P. F. Bedaque and U. van Kolck, arXiv:nucl-th/0203055.
- [25] S. Weinberg, *Phys. Lett. B.* **251**, 288 (1990).
- [26] S. Weinberg, *Nucl. Phys.* **B363**, 3 (1991).
- [27] S. Weinberg, *Phys. Lett. B.* **295**, 114 (1992).

- [28] S. R. Beane, C. Y. Lee, and U. van Kolck, Phys. Rev. C **52**, 2914 (1995).
- [29] M. Walzl and U. G. Meißner, Phys. Lett. **B513**, 37 (2001).
- [30] V. Bernard, N. Kaiser, and U.-G. Meißner, Int. Jour. of Mod. Phys. E **4**, 193 (1995).
- [31] J. Adam and H. Arenhövel, Nucl. Phys. **A614**, 289 (1997).
- [32] M. J. Savage, K. A. Scadferri, and M. B. Wise, Nucl. Phys. **A652**, 273 (1999).
- [33] J.-W. Chen, G. Rupak, and M. Savage, Nucl. Phys. **A653**, 386 (1999).
- [34] This peculiarity occurs because we pull out a factor of e when defining the operators \mathcal{O}_μ . If we counted $e \sim P$ then the counting for vertices involving photons would be exactly as for pion-nucleon interactions.
- [35] D. O. Riska, Prog. Part. Nucl. Phys. **11**, 199 (1984).
- [36] In terms of the notation of Ref. [44] the result (28) corresponds to $\tilde{\mu} = -1$. This occurs because the field-theoretic manipulations used to arrive at Eq. (28) assume that the fields represent physical particles, i. e. they are on-shell. This choice has been the standard one for computing χ PT kernels for interactions with light nuclei, see, e.g. [54, 55].
- [37] T.-S. Park, D.-P. Min, and M. Rho, Nucl. Phys. **A596**, 515 (1996).
- [38] T.-S. Park, K. Kubodera, D.-P. Min, and M. Rho, Phys. Lett. **B472**, 232 (2000).
- [39] E. Epelbaum, W. Glöckle, and U.-G. Meißner, Nucl. Phys. **A671**, 295 (2000).
- [40] D. R. Entem and R. Machleidt, Phys. Lett. **B524**, 93 (2002).
- [41] D. R. Phillips and T. D. Cohen, Nucl. Phys. **A668**, 45 (2000).
- [42] V. G. J. Stoks, R. A. M. Klomp, M. C. M. Rentmeester, and J. J. de Swart, Phys. Rev. C **48**, 792 (1993).
- [43] J. L. Friar, Phys. Rev. C **22**, 796 (1980).
- [44] J. Adam, H. Goller, and H. Arenhövel, Phys. Rev. C **48**, 470 (1993).
- [45] J. L. Forest, Phys. Rev. C **61**, 034007 (2000) [arXiv:nucl-th/9905063].
- [46] V. Bernard, N. Kaiser, J. Kambor and U. G. Meißner, Nucl. Phys. B **388**, 315 (1992).
- [47] B. Kubis and U. G. Meißner, Nucl. Phys. A **671**, 332 (2000) [Erratum-ibid. A **692**, 647 (2001)] [arXiv:hep-ph/9908261].

- [48] V. Bernard, H. W. Fearing, T. R. Hemmert and U. G. Meißner, Nucl. Phys. A **635**, 121 (1998) [Erratum-ibid. A **642**, 563 (1998)] [arXiv:hep-ph/9801297].
- [49] P. Mergell, U. G. Meißner and D. Drechsel, Nucl. Phys. A **596**, 367 (1996) [arXiv:hep-ph/9506375].
- [50] G. G. Simon and C. Schmitt and V. H. Walther, Nucl. Phys. **A364**, 285 (1981).
- [51] S. Auffret *et al.*, Phys. Rev. Lett. **54**, 649 (1985).
- [52] R. Cramer *et al.*, Z. Phys. **C29**, 513 (1985).
- [53] R. Schiavilla and I. Sick, Phys. Rev. C **64**, 041002 (2001) [arXiv:nucl-ex/0107004].
- [54] S. R. Beane *et al.*, Nucl. Phys. **A618**, 381 (1997).
- [55] S. R. Beane, M. Malheiro, D. R. Phillips, and U. van Kolck, Nucl. Phys. **A656**, 367 (1999).